Results from Mexnext:

Analysis of detailed aerodynamic measurements on a 4.5 m diameter rotor placed in the large German Dutch wind tunnel DNW

J.G. Schepers, K. Boorsma, A. Bon, C. Kim and T. Cho

Results from Mexnext: Analysis of detailed aerodynamic measurements on a 4.5 m diameter rotor placed in the large German Dutch Wind Tunnel DNW

J.G. Schepers, K. Boorsma and A. Bon
The Energy Research Centre of the Netherlands
schepers@ecn.nl, boorsma@ecn.nl, bon@ecn.nl

C. Kim and T. Cho
Korea Aerospace Research Institute, KARI
cwkim@kari.re.kr, cho@ecn.nl

Abstract

This paper presents an analysis of measurements which have been taken in the EU project Mexico (Model Rotor Experiments In Controlled Conditions). In the Mexico project a large number of European research institutes and universities cooperated. The project resulted in a database of measurements on a 3 bladed 4.5 m diameter wind turbine model placed in the LLF tunnel (with a 9.5 by 9.5 m^2 open test section) of DNW in the Netherlands. Pressure and load measurements on the blade have been carried out simultaneously with stereo PIV flow field measurements.

An extensive analysis of the Mexico measurements takes place within IEA Task 29 Mexnext. The paper presents recent results from this project where special attention is paid to the influence of the rotational speed on the aerodynamic blade loads (where results from a scaled down Mexico rotor as built by KARI are also shown), the flow near the tip of the blade (the analysis of which is supported by results from a free wake lifting line code) and a comparison between calculated and measured results.

Keywords: wind turbine aerodynamics, wind tunnel measurements,

1   Introduction

The paper will present the most recent results from IEA Task 29 Mexnext. Mexnext is a joint project in which 20 parties from 11 different countries cooperate:

- Canada (École de technologie supérieur, Montréal (C. Masson, S. Breton, C. Sibuet), and University of Victoria (C. Crawford))
- Denmark (RISØ-DTU (H. Madsen and N. Sørensen) and DTU-MEK (W. Z. Shen))
- Germany(University of Stuttgart (T. Lutz, K. Meister), University of Applied Sciences at Kiel (P. Schaffarczyk and A. Jeromin), ForWind (B. Stoevesandt))
- Israel (Technion (A. Rosen, V. Ognev. R. Gordon))
- Japan (Mie University/National Institute of Advanced Industrial Science. (T. Maeda, Y. Kamada, J. Murata)
- Korea (Korea Institute of Energy Research KIER, (H. Shin) and Korea Aerospace Research Institute, KARI (C. Kim, T. Cho))
- Netherlands (ECN (G. Schepers, K. Boorsma, H. Snel), TUDelft (N. Timmer, D. Micallef), Suzlon Blade Technology (A. Verhoeff), TUTwente (E. van der Weide)
- Norway (Institute for Energy Technology/Norwegian University of Science and Technology (A. Knauer, J. van Rij))
- Spain (CENER (X. Munduate, S. Gomez) and INTA (C. Redonde))
- Sweden (Royal Institute of Technology/University of Gotland (S. Ivanell and K. Nilsson))
- USA (National Renewable Energy Laboratory, (S. Schreck))

The Mexnext project started on June 1, 2008 and will end on June 1, 2011 The main aim of Mexnext is to analyse the wind tunnel measurements which have been taken in the EU project Mexico [1]. In the Mexico project (which ended in February 2007) 10 institutes from 6 countries cooperated in doing experiments on an instrumented, 3 bladed wind turbine of 4.5 m diameter placed in the 9.5 by 9.5 m^2 open section of the Large Low-speed Facility (LLF) of DNW in the Netherlands. A tapered,

twisted blade was used with three different aerodynamic profiles (DU91-W2-250, RISØ-A1- 21 and NACA 64-418). The blades were tripped at 5% chord at suction and pressure side to avoid possible laminar separation phenomena.

Figure 1: Setup of model turbine in the Measurement Section of the DNW LLF

Pressure distributions on the blades were obtained from 148 Kulite absolute pressure sensors, distributed over 5 sections at 25, 35, 60, 82 and 92 % radial position respectively. Blade loads were monitored through two strain-gauge bridges at each blade root. Pressures and strains were sampled with 5.5 kHz effectively, after filtering. Furthermore tower foot moments have been measured. Most interesting however are the extensive flow field measurements, which have been taken simultaneous to the pressure and load measurements.

The Mexico database covers conditions which represent the entire operational regime of a wind turbine: Measurements have been done at two rotational speeds, several tunnel speeds, several pitch angles and several yaw angles (including zero yaw). More specifically: The rotational speed was either 424 rpm or 324 rpm which corresponds to tip speeds of 76 m/s and 100 m/s respectively. At 424 rpm a chord based Reynolds number of approximately 0.8 M was reached without entering into noticeable compressible conditions (Mach ≈ 0.3); The tunnel speeds ranged between 10 m/s and 30 m/s which made it possible to cover tip speed ratios between 3.3 and 10. The design tip speed ratio is 6.7 which corresponds to a tunnel velocity of 15 m/s and a rotor speed of 424 rpm. The design pitch angle was -2.3 degrees. All results presented in this paper are taken at this pitch angle.

2 Results

Previous results of analyses have been described in [2], [3], [4] and [5]. Most of the present analyses focus on new studies, in particular:
- The influence of rotational speed on several aerodynamic coefficients.
- The flow field near the tip.
- A comparison of Mexico measurements and calculated results from several codes

2.1 Influence of rotational speed

The influence of rotational speed on the aerodynamic coefficients was already addressed in [5] where results have been presented in terms of axial force coefficients as function of tip speed ratio, see figure 2. In this way of presenting, the axial force (coefficient) is expected to be independent of the rotational speed. Nevertheless some differences from the rotational speed could still be possible through the Reynolds influence and/or different rotational (3D) effects on the airfoil data. The axial force coefficients from figure 2 are determined with two independent measurement techniques. The first technique uses the axial force as measured with the balance at the tower foot where a correction for tower drag has been applied to determine the rotor axial force. Note that the tower drag could be determined from the tower foot axial force and fore-aft moment by assuming a uniform tower drag.

The second technique is based on integrating the axial force distribution along the blade as found from the pressure distributions at the 5 instrumented sections. The first observation on figure 2 is that the differences between the 'pressure' and 'balance' axial force are very small giving confidence in both the pressure and balance measurements. A second observation is that the dependency of axial force coefficient on the rotational speed is limited in this region.

Another indication for the rotor speed sensitivity is found by comparing the power coefficients C_P as function of tip speed ratio. Thereto it should be realised that the axial force coefficients from figure 2 are mainly influenced by the lift coefficients, but the power coefficients are also influenced by the drag coefficients which are generally more sensitive to Reynolds number effects. Unfortunately the power has not been measured directly on the Mexico rotor. An attempt was made to derive the rotorshaft torque from the moments and loads at the tower
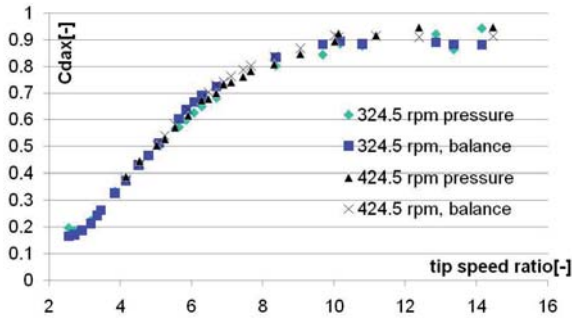
Figure 2: Axial force coefficient from pressure distributions and balance as function of tip speed ratio for two rotational speeds: 324.5 and 424.5 rpm.

foot balance according to:

$$M_{torq,rotor} = M_{torq,balance} - F_{lat,balance} \cdot towerheight$$
(1)

The rotorshaft torque obtained in this way was found to be fully rotational speed independant but nevertheless the results were believed to be unrealistic in view of a large lateral balance force even at non-yawed conditions. For this reason the rotor shaft torque has also been derived from the pressure forces even though it is acknowledged that this excludes the effect of viscous drag, which is one of the main drivers for a Reynolds number dependancy.

The power coefficients as derived from these rotor shaft torque values at 324 and 424 rpm could be compared with measurements at different rotational speeds which have been taken on a 'daughter' of the Mexico rotor. This daughter has been built by KARI and it is a perfect look alike of the Mexico rotor but scaled down to a rotor diameter of 2 meter. The model is placed in an open measurement section of a KARI wind tunnel with a size of 5 x 3.75 m^2, where the Mexico rotor has a diameter of 4.5 m and was placed in an open measurement section with a size of 9.5x9.5 m^2. The test was conducted at various tip speeds, including the value of 76 m/s, which was used in the Mexico test. The maximum tip speed was 90 m/s (where the maximum tip speed in the Mexico experiment was 100m/s). Transition was fixed at 5% chord line at both the suction and pressure side, to match the Mexico experiment. The torque was directly measured with a torque sensor installed in the rotating axis. In figure 4 the power coefficient as function of tip speed ratio is compared for the KARI and Mexico experiment at tip speeds of 76 m/s and 90 m/s (KARI) and 100 m/s (Mexico). The maximum C_P is found near a tip speed ratio of 6.6 (as expected)

and the influence of rotational speed is generally small. The $C_{P,max}$ of the KARI wind turbine ≈ 0.33 which is lower than the $C_{P,max} \approx 0.38$ of the Mexico rotor. A lower value for the KARI rotor could be expected, in view of its lower Reynolds number with high drag values: The Reynolds number near the tip of the KARI rotor varies between 1.8 to 3.2 10^5, where the Reynolds number near the tip of the Mexico rotor varies roughly between 6 and 8 10^5. Apart from this the neglect of viscous drag in the Mexico results will lead to a higher power coefficient. At low tip speed ratios (large angles of attack) pressure drag will be dominant above viscous drag but at high tip speed ratios the contribution of viscous drag is larger.

In figure 5 the KARI measurements at 5 different rotational speeds are presented in terms of a torque coefficient using the blade tip speed as a reference velocity in order to compare the test results for various rotating speeds:

$$C_{torque} = \frac{Torque}{0.5\rho V_{tip}^2 \pi R^3} = \frac{C_P}{\lambda^3}$$
(2)

The KARI measurements at low tip speeds (50 to 70 m/s) do indicate a clear rotor speed dependency in particular near stall ($\lambda \approx 4$, i.e $\lambda^{-1} \approx 0.25$ in figure 5). The explanation for the relatively strong rotor speed dependency in the KARI experiments at low rotational speeds might be the smaller size and resulting lower Reynolds number since the Reynolds number sensitivity is known to be strongest at low values of the Reynolds number.

Figure 3: KARI wind tunnel with scaled down model of Mexico rotor, compare with figure 1

2.2 Tip flow

Figure 6 shows the axial velocities in the viscinity of the rotor plane over an axial distance from approximately 0.3 m upstream of the rotor to approximately 0.3 m downstream of the rotor at r/R
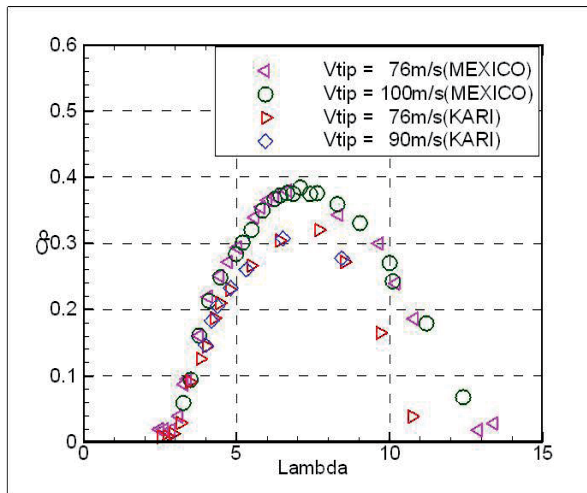
Figure 4: Power coefficients as function of tip speed ratio for KARI and Mexico experiment at different tip speeds

Figure 5: Torque coefficient as function of (tip speed ratio)$^{-1}$ for KARI experiment

= 0.8. These flow traverses have been made by combining 2 PIV sheets, one sheet upstream of the rotor plane and another sheet downstream of the rotor plane, with a small overlap in the rotorplane. The PIV sheets are located in a horizontal plane at the 9 o' clock position (270 degrees azimuth). The measurements have been done at design conditions (V_∞ = 15 m/s) at different blade positions, the legend of them is given in figure 7, see also [5] for more information on the measurement procedure. Note that the positions in figure 7 refer to the blade which is denoted as blade number 1.

The measurements are compared with calculations from the program AWSM, which is a free wake lifting line method from ECN, see [6]. From these measurements (and calculations), an idea can be formed of the flow non-uniformity between the rotor blades from which the validity of the Prandtl tip correction can be assessed. The Prandtl tip correction is the generally applied correction for this non-uniformity in BEM based codes. It is defined as the ratio between the annulus averaged induction factor and the local axial induction at the blade.

The first observation which can be made is that generally speaking the agreement between the measured and AWSM calculated velocities is very good. An abrupt change in velocity is visible in both calculations and measurements when blade 1 moves from 20 to 40 degrees, i.e. when blade 3 moves from 260 to 280 degrees and crosses the PIV sheet. The abrupt change is a result of the upwash (ie. the velocity induced by the bound vortex strength) which adds a positive component to
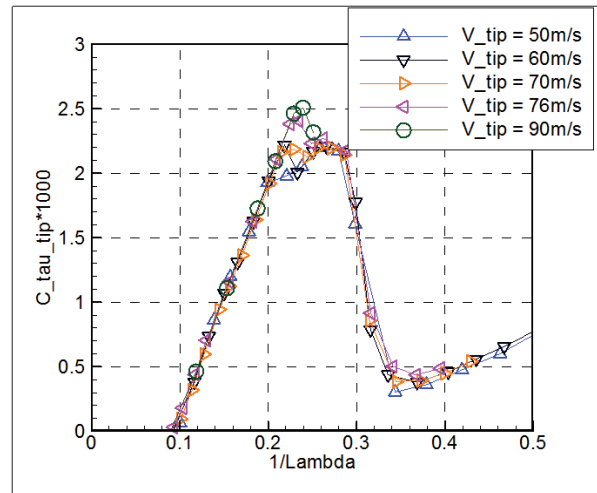
the axial velocity at 260 degrees and a negative component at 280 degrees, see also [5]. It can be noted that the agreement between the AWSM results and measurements is poorest at these blade positions. This can be explained by the lifting line approximation in AWSM which in the vicinity of the blade leads to a poor representation of the flow around the actual blade geometry.

Note that this non-uniformity from the bound vortex (which also plays a role at the other blade positions) is not considered in the Prandtl tip correction.

Now a further analysis takes place of the flow non-uniformity in the rotor plane (i.e. at x = 0 m). The traverses as presented in figure 6 have been made at 6 different blade positions but none of them correspond to 270 degrees, i.e. the position where the blade is in the PIV sheet. Such measurements are however available from another type of experiment, the so-called tip vortex tracking experiments, see e.g. [2], where the flow field was measured near the blade tip at a blade position of 270 degrees.

Then the figures 8 to 10 show velocity measurements near the tip in the rotor plane at V=10, 15 and 24 m/s. The figures show both the azimuthally averaged velocities as well as the local velocities with the blade at a position of 270 degrees. It is recalled that the ratio between the azimuthally averaged induced velocity and the local induced velocity is the Prandtl tip correction. The measured results are compared with those calculated with AWSM. The azimuthally averaged measured values are averaged over the 6 blade positions from figure 7 where the AWSM calculations are aver-
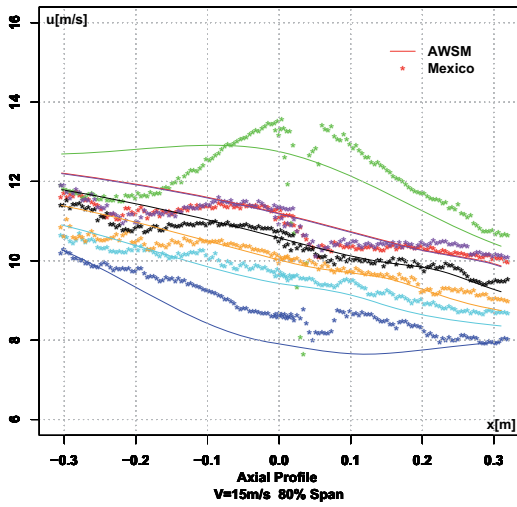
Figure 6: Axial traverse near the rotor at 80% span and V_∞ = 15 m/s, different blade positions, see figure 7. Measured and calculated with AWSM
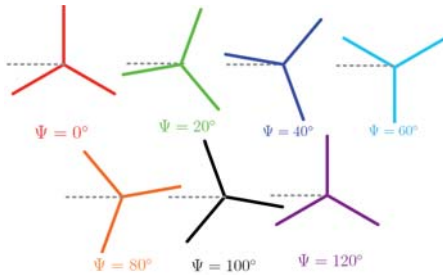

Figure 7: Position of the blades for $\Psi \in \{0; 20; 40; 60; 80; 100; 120\}°$

aged over 12 blade positions.

It should be known that the results from the figures 8 to 10 are derived from data which include the upwash from the bound vortex. At first sight one may think that this makes the results inapplicable for an assessment of the Prandtl tip correction since, as stated above, this upwash is not included in the Prandtl tip correction. However, the present way of processing filters out the effect from the upwash. This is due to the fact that the data are azimuthally averaged over different blade positions which are all symmetrically positioned around the PIV sheet at 270 degrees. As an example: the upwash at 280 degrees is opposite to the upwash at 260 degrees (at least when the bound vortex is thought to be concentrated in a vortex line). Also the local axial induction factor, i.e. the result with the blade at 270 degrees, is not disturbed by this upwash since

the bound vortex at this position does not induce a velocity in axial direction.

An important observation from the figures 8 to 10 is the very good agreement between measured and AWSM predicted azimuthally averaged velocities in the rotor plane.

Another observation is the good qualitative agreement between the calculated and measured local velocities where the drop in velocity followed by an increase in velocity towards the tip, which is a result from the tip vortex (see below), is present in both calculations and measurements. It is noted however that the increase in velocity takes place at a more inboard position than predicted by AWSM. This is a result of the fact that the so-called tip vortex tracking experiments showed that the tip vortex is trailed slightly inboard from the tip where AWSM assumes this vortex to be trailed at the tip. Furthermore it can be seen that the measured velocities are lower at r < R and they do not tend to coincide with the azimuthally averaged velocity at more inboard positions as can be seen in the AWSM results. This would also be expected from the Prandtl tip loss factor which approaches a value of 1 at inboard positions, which implies the azimuthally averaged velocity to be equal to the local velocity at the blade. Possibly the velocity is not measured precisely at the blade position because the 1P trigger sensor (from which the blade position is derived) was sometimes found to behave unstable during the experiments. Since the velocities local to the blade are very sensitive to the precise value of the blade position the results can be disturbed heavily by a relatively small offset in position. Another explanation could be the fact that AWSM applies 2D airfoil coefficients over the entire blade where the actual airfoil coefficients on a rotating blade are known to be much lower, see e.g. [7].

Nevertheless the comparison between AWSM results and measurements is considered convincing enough to propose a lifting line free vortex wake method as a basis for a refinement of the tip loss factor. Thereto it should be realised that the Prandtl tip loss factor has been determined in the pre-computer era (1919) with a very simplified vortex wake model but nowadays a modern vortex wake method like AWSM could be used for a more physical estimate for the tip loss factor.

In the figures 11 to 13 the tip loss factors from AWSM (i.e. the ratio between the azimuthally averaged induction factor and the local induction factor) are compared with the Prandtl tip loss factors. Most interesting is the behaviour of these factors

near the tip (the wiggles at the mid-span positions are most likely a result of intermediate vortex shedding). Generally speaking the AWSM tip loss factor follows the Prandtl tip loss factor very closely but the AWSM tip loss factor is higher at high tip speed ratio (10 m/s) and lower at low tip speed ratio (24 m/s) At the intermediate wind speed of 15 m/s a good agreement is found. This might indicate that the tip speed ratio dependency (i.e. the inflow angle dependency) in the Prandtl tip loss correction factor could be improved. This will be done in future research.

A striking difference between the Prandtl tip loss factor and the ASWM tip loss factor can be seen at the very tip. The Prandtl tip loss factor decreases to 0 but the AWSM factor increases before the tip. This is consistent with the results from the figures 8 to 10 which show that the local blade velocity exceeds the azimuthally averaged velocities already inboard from the tip. In order to understand this, it needs to be realised that the AWSM tip vortex is a singularity which in principle yields an infinite induced velocity and hence an infinite decrease of total velocity towards the tip. This however assumes the flow to be inviscid where viscosity will prevent such a singularity to exist in the real flow. Consequently AWSM applies a so-called cut-off radius, the default value of which is 5%. This means that if the distance between a point and a segment of the wake is less than 5% of the segment length, the velocity induced by the segment is neglected. As a result of this cut-off radius, the velocity local to the blade increases towards the tip.

A sensitivity study showed only a significant effect of the cut-off radius at the very tip, i.e. at the outer 2% of the radius. Together with the fact that the qualitative agreement between the AWSM results with 5% cut-off radius and measured results is good, it is believed that AWSM with this default cut-off radius can be used with sufficient confidence for a better assessment of the tip loss effects.

Another interesting observation is the behaviour of the loss factor near the root. In the figures 11 to 13 the Prandtl tip loss factor has, despite the name **tip** loss factor, also been applied at the root. Thereto the tip radius in the original tip loss factor has been replaced by a root radius which is obviously less well defined than the tip radius. In the figures 11 to 13 the root radius has been set as the location of the maximum chord which seems to be a reasonable choice.
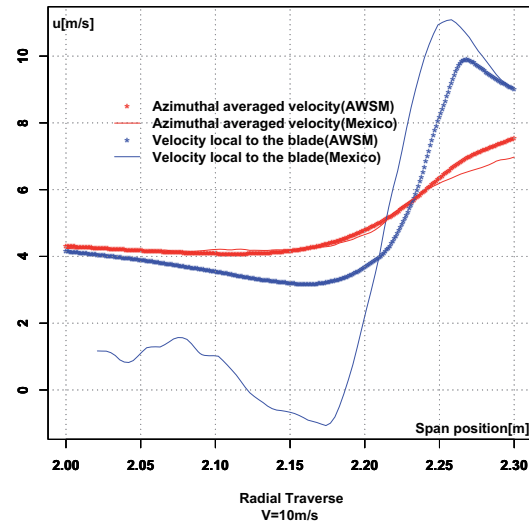

Figure 8: Local and azimuthally averaged velocities in the rotor plane, measured and AWSM calculated, V = 10 m/s

2.3 Comparison between measurements and simulations

In this section some comparisons are shown between Mexico measured results and calculated results. The calculations are performed by the participants in the Mexnext project. Most interesting in this comparison is the fact that the comparison is not only made with load measurements but also with the underlying flow field measurements which drive these loads. A comparison between Mexico flow field data and CFD data can be made straightforwardly but a comparison with BEM data is obscured by the fact that the flow model in the momentum theory is of a very simplified nature: It only considers the induced velocities in the rotor plane and far downstream where the rotor is represented by a hypothetical actuator disc. Hence the induced velocity in the actuator disc plane is not a real physical quantity which can be compared directly with the measured quantity since it does not include the upwash from the blade and the flow non-uniformity due to the finite number of blades (see section 2.2).

Before discussing the comparison between calculated and measured results a qualitative discussion of some measured results may aid the interpretation.

In figure 14 the axial velocity decay at 61% and 82% span is presented for design conditions. These measurements are again done in a horizontal plane at the 9 o' clock position in a phase locked
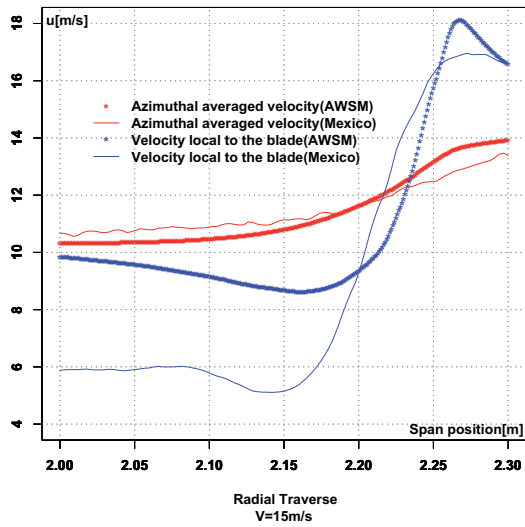
Figure 9: Local and azimuthally averaged velocities in the rotor plane, measured and AWSM calculated, V = 15 m/s

Figure 10: Local and azimuthally averaged velocities in the rotor plane, measured and AWSM calculated, V = 24 m/s

way i.e. the results are averaged over a number of samples which are all taken at a blade position of 0 degrees. The results are averaged over the axial extent of the PIV sheet.

Also indicated are the results from a cylindrical vortex wake method. This model is based on an actuator disc approach with a constant bound vortex strength over the disc which yields $C_{Dax} = 4a_{rotor}(1-a_{rotor})$ and $a_\infty = 2 a_{rotor}$, with a_{rotor} the axial induction factor in the rotor plane and a_∞ the axial induction factor very far downstream of the rotor. This makes the results from this cylindrical vortex sheet method compatible to the results from the momentum theory but the advantage of the cylindrical vortex wake model lies in the fact that the entire velocity decay from x = -∞ to x = +∞ is covered.

The axial force coefficient in the cylindrical vortex sheet method was set to 0.89 which was beforehand the expected value in view of the fact that these measurements are performed at design conditions.

Figure 14 has already been discussed in [5], where it is explained that generally speaking a good agreement is found between the measured decay and the decay from the cylindrical vortex wake model. This is in particular true at the locations upstream of the rotor plane and in the far wake. It is anyhow encouraging to see that generally speaking the velocity defect far downstream is approxi-
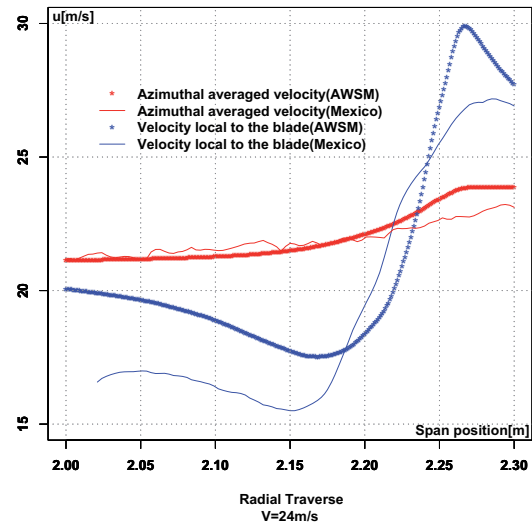
mately twice the velocity defect in the rotor plane in agreement with the assumptions in the momentum theory. Furthermore the velocity defect is rather independent of radial position, which confirms the 1D assumption from the momentum theory.

The discrepancies near the rotor plane are partly explained by the actuator disc assumption in the cylindrical vortex wake model which, as stated above, implies a uniform flow in the rotor plane, opposite to the real flow field situation where non-uniformities exist due to the finite number of blades.

The fluctuations at 61% span are most likely due to the transition in airfoils leading to a change in bound vortex strength near this location. They cannot be reproduced since the model assumes a constant bound vortex strength along the blade.

Hence the measured velocity decay seems to agree reasonably well with the momentum theory if C_{Dax} is set to the expected value of 0.89 but it was then very striking to note that the measured C_{Dax} is only 0.72, see figure 2. Such low C_{Dax} yields much lower axial induced velocities and hence a higher velocity level. The first logical thought would be that the C_{Dax} measurements from figure 2 are incorrect but this is difficult to believe in view of the fact that these values are determined with two fully independent measurement techniques, the results of which agree very well at all datapoints at different tunnel speeds and different rotational speeds.
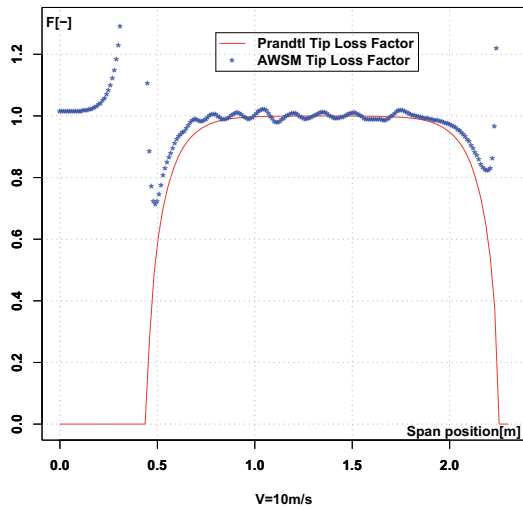
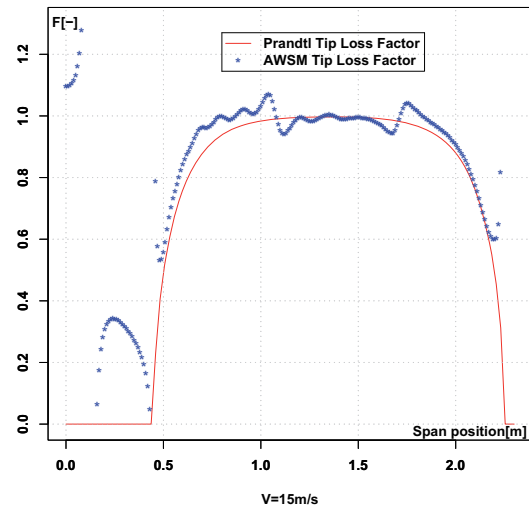Figure 11: Prandtl tip loss correction compared with AWSM tip loss factor, V = 10 m/s

Figure 12: Prandt tip loss factor compared with AWSM tip loss factor, V = 15 m/s

Another explanation for the anomalies could be tunnel effects. An extensive investigation on the impact of these effects takes place within the Mexnext project on basis of CFD calculations, see also [4]. Until now the impact of these effects seems to be small at design conditions, and the limited effect which has been found points in the opposite direction: When the induction in the tunnel is the same to the induction in the free stream, the C_{Dax} is higher in the tunnel situation. This implies that the free stream C_{Dax} would even be lower than 0.72.

As such an explanation for the discrepancy between measurements and momentum theory has not been found yet but the logical consequence is that none of the calculations from the Mexnext group can predict both the velocities AND loads in a correct way: The calculations overpredict the velocity (underpredict the induction) and/or overpredict the loads. This is clearly visible in the figures 15 to 17. They show results from several CFD calculations for the normal force distribution along the blade and the radial and axial traverses of the axial velocity in comparison with the measurement. As a matter of fact all codes overpredict both the loads and the velocities. Nevertheless the results of some codes approach the measurements very closely but this is only true for either the velocities or the loads. Despite these discrepancies it is very encouraging to see the good qualitative agreement between calculations and measurements also in terms of flow details: Figure 16 shows the increase

in normal force along the radius (i.e. $\frac{dF_n}{dr}$) to be predicted well. Figure 15 generally shows a good qualitative prediction of the velocity decay despite the off-set in velocity level.

Furthermore figure 17 shows, in both measurements and calculations a lower velocity in the centre of the wake where the velocity increases near the edge of the wake (i.e. near r ≈ 2.25 m). This increase is associated to the presence of the tip vortex. Many codes predict the increase in velocity to be less abrupt than the measured increase. The significant drop in velocity towards the inboard positions is most likely a result of the vorticity due to the transition in airfoils which, as stated above, leads to a change in bound vortex strength along the blade. Apparently this drop cannot be reproduced by none of the codes.

3   Conclusion

The main conclusions from the investigations presented in this paper are:
○ The effect of rotor speed on aerodynamic coefficients is very limited in the Mexico rotor. For the smaller KARI rotor at low rotational speed a rotor speed dependancy is visible near stall.
○ The velocities as measured near the tip show a behaviour consistent with the concept used in the Prandtl tip loss factor and with results from a free wake lifting line method. The comparison with the free wake lifting line method indicates that the dependency of the Prandtl tip loss factor
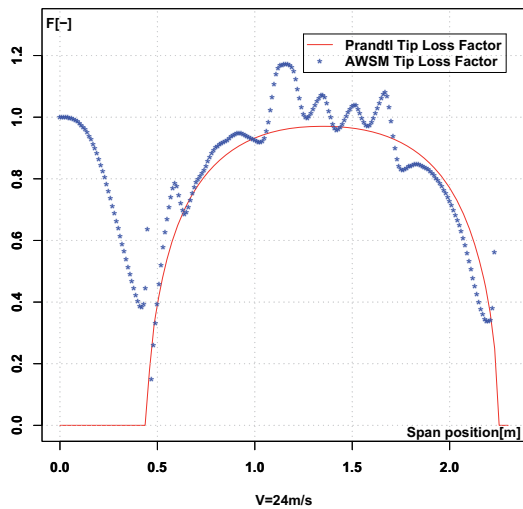
Figure 13: Prandt tip loss factor compared with AWSM tip loss factor, V = 24 m/s

Figure 14: Axial velocity decay at V = 15 m/s
Y = 1,374m (61% span),
Y = 1,845m (82% span),
Cylindrical vortex wake method

on inflow angle can be improved. This will be done in future research when also the tangential induced velocities will be considered.

○ The PIV measurement do confirm some expectations from the momentum theory: The velocity defect far downstream is twice the velocity defect in the rotor plane. Moreover, with the exception of the velocities in the rotor plane, the velocity decay is independent of radial position.

○ A striking observation is the fact that the measured velocity decay at design conditions agrees well with the velocity decay from the momentum theory as long as the axial force coefficient is set to the expected value of 0.89. The measured axial force coefficient however only amounts to 0.72! Until now all investigations on measurement quality indicate that the measurements are accurate where tunnel effects point in an opposite direction. More research on an explanation for this observation will be carried out because it is difficult to believe in a very fundamental flaw in the momentum theory. It anyhow implies that none of the calculations predict both the velocities as well as the loads fully correct. Despite these discrepancies the overall agreement between calculations and measurements is very encouraging also in terms of flow details, for which the Mexico project provided very unique information.

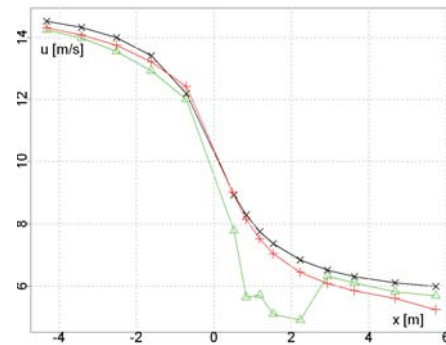## References

[1] J.G. Schepers and H. Snel. "Mexico, Model experiments in controlled conditions". ECN-E-07-042, Energy Research Center of the Netherlands, 2007.

[2] H. Snel, J.G. Schepers and A. Siccama. "Mexico, the database and results of data processing and analysis ". In *47th AIAA Aerospace Sciences meeting*, January 2009.

[3] H. Snel, J.G. Schepers and B. Montgomerie. "The Mexico project (Model experiments in controlled condition). The database and first results of data processing and interpretation". In *Proceedings of EAWE conference 'The Science of Making Torque from the Wind'*, 2007.

[4] J.G. Schepers, H. Snel and K. Boorsma. "IEA Task 29 Mexnext: Analysis of wind tunnel measurements from the EU project Mexico". In *Proceedings of EAWE conference 'The Science of Making Torque from the Wind'*, June 2010.

[5] J.G. Schepers, L. Pascal and H. Snel. "First results from Mexnext: Analysis of detailed aerodynamic measurements on a 4.5 m diameter rotor placed in the large German Dutch Wind Tunnel DNW". In *Proceedings of European Wind Energy Conference, EWEC*, April 2010.

[6] A. van Garrel. "Development of a wind turbine aerodynamics simulation module". ECN-C–03-079, Energy Research Centre of the Netherlands, ECN, August 2003.

[7] J.G. Schepers, L. Feigl, R. van Rooij and A. Bruining. "Analysis of detailed aerodynamic measurements, using results from an aeroelastic code ". In *Wind Energy Journal 7:'*, pages 357–371, August 2004.
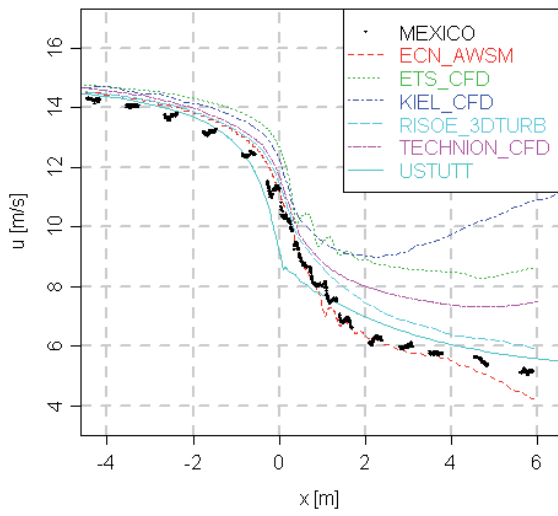
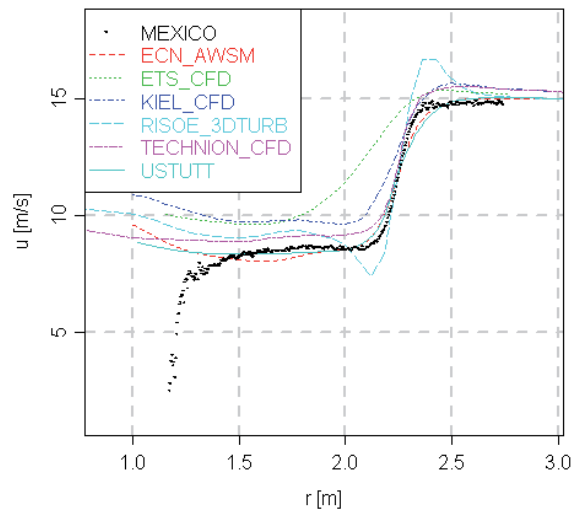Figure 15: Axial velocity decay, measured and calculated with CFD codes, V = 15 m/s

Figure 17: Radial traverse of axial velocities, 30 cm downstream of the rotor, measured and calculated with CFD codes, V = 15 m/s, blade position is 60 degrees, see figure 7
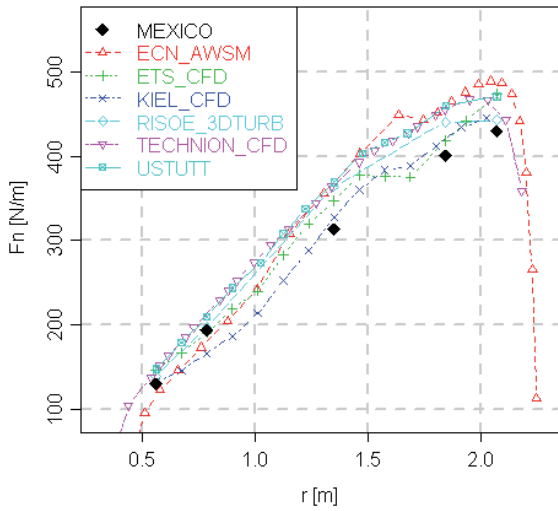

Figure 16: Normal force distribution along the blade, measured and calculated with CFD codes, V = 15 m/s